Journal for ImmunoTherapy of Cancer

Extensive-stage small-cell lung cancer in patients receiving atezolizumab plus carboplatin–etoposide: stratification of outcome based on a composite score that combines gene expression profiling and immune characterization of microenvironment

Anna Tosi,[1] Martina Lorenzi,[2] Paola Del Bianco,[3] Anna Roma,[4] Alberto Pavan,[5] Antonio Scapinello,[6] Maria Vittoria Resi,[7] Laura Bonanno ,[8] Stefano Frega,[8] Fiorella Calabrese,[9] Valentina Guarneri,[7,8] Antonio Rosato,[1,7] Giulia Pasello [7,8]

To cite: Tosi A, Lorenzi M, Del Bianco P, *et al*. Extensive-stage small-cell lung cancer in patients receiving atezolizumab plus carboplatin–etoposide: stratification of outcome based on a composite score that combines gene expression profiling and immune characterization of microenvironment. *Journal for ImmunoTherapy of Cancer* 2024;**12**:e008974. doi:10.1136/jitc-2024-008974

► Additional supplemental material is published online only. To view, please visit the journal online (https://doi.org/10.1136/jitc-2024-008974).

AT and ML are joint first authors.

AR and GP are joint senior authors.

Accepted 13 June 2024

Check for updates

© Author(s) (or their employer(s)) 2024. Re-use permitted under CC BY-NC. No commercial re-use. See rights and permissions. Published by BMJ.

For numbered affiliations see end of article.

Correspondence to
Dr Giulia Pasello;
giulia.pasello@iov.veneto.it

ABSTRACT

Purpose Small-cell lung cancer (SCLC) is an aggressive disease with a dismal prognosis. The addition of immune checkpoints inhibitors to standard platinum-based chemotherapy in first-line setting achieves a durable benefit only in a patient subgroup. Thus, the identification of predictive biomarkers is an urgent unmet medical need.

Experimental design Tumor samples from naive extensive-stage (ES) SCLC patients receiving atezolizumab plus carboplatin–etoposide were analyzed by gene expression profiling and two 9-color multiplex immunofluorescence panels, to characterize the immune infiltrate and SCLC subtypes. Associations of tissue biomarkers with time-to-treatment failure (TTF), progression-free survival (PFS) and overall survival (OS), were assessed.

Results 42 patients were included. Higher expression of exhausted CD8-related genes was independently associated with a longer TTF and PFS while increased density of B lymphocytes correlated with longer TTF and OS. Higher percentage of M2-like macrophages close to tumor cells and of CD8+T cells close to CD4+T lymphocytes correlated with increased risk of TF and longer survival, respectively. A lower risk of TF, disease progression and death was associated with a higher density of ASCL1+tumor cells while the expression of POU2F3 correlated with a shorter survival. A composite score combining the expression of exhausted CD8-related genes, B lymphocyte density, ASCL1 tumor expression and quantification of CD163+macrophages close to tumor cells, was able to stratify patients into high-risk and low-risk groups.

Conclusions In conclusion, we identified tissue biomarkers and a combined score that can predict a higher benefit from chemoimmunotherapy in ES-SCLC patients.

WHAT IS ALREADY KNOWN ON THIS TOPIC

⇒ The identification of predictive biomarkers of durable benefit from chemoimmunotherapy in extensive-stage small-cell lung cancer (SCLC) is an urgent unmet medical need.

WHAT THIS STUDY ADDS

⇒ The present study integrates information from gene expression profiling, cell phenotype analysis and the measurement of spatial cell distribution to define a combined predictive and prognostic factor capable of stratifying high-risk and low-risk patients.

HOW THIS STUDY MIGHT AFFECT RESEARCH, PRACTICE OR POLICY

⇒ The combined score may give a complete overview of the immunogenic features of each cancer leading to the identification of outliers SCLC patients in the clinical practice.

INTRODUCTION

Small-cell lung cancer (SCLC) is an aggressive disease with poor prognosis, accounting for approximately 15% of all lung cancers.[1] Most patients are diagnosed with an extensive-stage disease (ES).[2] Platinum-based chemotherapy has been the standard first-line treatment over the past 40 years[3]; however, after an initial response to treatment, progression typically occurs within 1 year.

Several studies have consistently shown that the addition of immune checkpoint inhibitors (ICIs) to standard chemotherapy improves survival, thus leading to a new standard first-line treatment in this setting.[4–8]

J Immunother Cancer: first published as 10.1136/jitc-2024-008974 on 1 July 2024. Downloaded from http://jitc.bmj.com/ on December 31, 2024 by guest. Protected by copyright.

In the randomized phase III IMpower-133 trial, the addition of atezolizumab to standard chemotherapy showed a significant improvement in median overall survival (mOS) from 10.3 to 12.3 months compared with chemotherapy alone, with a manageable safety profile.[5] Similarly, the CASPIAN trial showed an mOS improvement with the addition of durvalumab to chemotherapy (12.9 months) compared with chemotherapy alone (10.5 months).[4 9]

However, durable benefit occurs in about 15% of patients.[5] Several predictive biomarkers have been investigated, but the prospective identification of patients more likely to have a better outcome appears challenging in SCLC.[9] Indeed, tissue samples are often scarce, the aggressive nature of the disease often precludes in-depth studies requiring surgical specimens, and classical immune-predictive biomarkers such as PD-L1 or tumor mutational burden (TMB) do not correlate with outcome.[7 10–16]

Tumor immune microenvironment (TME) of SCLC remains poorly understood and is commonly classified as "cold" lacking an infiltration of cytotoxic immune cells, notwithstanding the presence of high TMB.[17] While high TMB correlates with increased neoantigen production and favorable response to anti-PD-L1/PD1 in NSCLC,[18] this is not the case in SCLC.[11 16] These observations underscore the need to uncover the mechanisms restricting immune cell infiltration in SCLC to develop therapeutic approaches that warm up the immune landscape and to identify predictive biomarkers for patient selection.

Recently, a new molecular stratification of SCLC in four subtypes with different susceptibility to ICIs has been proposed, which is defined by differential expression of the transcription factors ASCL1, NEUROD1 and POU2F3, or low expression of all these three signatures accompanied by an inflammatory gene signature (SCLC-A, SCLC-N, SCLC-P and SCLC-I, respectively).[19 20] Beyond the intertumor heterogeneity, tumor cells may undergo a phenotypic switch or temporal evolution from one subtype to another, a typical hallmark called tumor plasticity.[21]

In this scenario, we identified immune-related biomarkers and a combined score predictive of outcome in ES-SCLC patients receiving chemoimmunotherapy, potentially useful for detecting early resistance and long-term benefit.

MATERIALS AND METHODS

Study design and eligibility criteria

This is a multicenter, translational, prospective study (CATS/ML43257 study) conducted in accordance with Good Clinical Practice guidelines and the Declaration of Helsinki.All ES-SCLC patients eligible for first-line treatment with carboplatin–etoposide plus atezolizumab were enrolled.

The primary endpoint was the correlation of gene expression profile (GEP) and TME with time-to-treatment failure (TTF). Secondary endpoints were the correlation of GEP and TME with progression-free survival (PFS) and OS, the identification of a composite score to better stratify patient outcome, and the description of GEP and TME in specific molecular subsets.

Eligible patients received an induction phase of carboplatin plus etoposide and atezolizumab for four cycles, followed by maintenance atezolizumab until unacceptable toxicity, disease progression or loss of clinical benefit, at the dose regimen detailed in figure 1. CT scans of the brain, chest and abdomen for tumor assessment were performed at the baseline and every three cycles. Clinical and pathological characteristics of the patients were recorded in an electronic case report form, and a dedicated anonymized database was updated until the last follow-up or death from any cause.

Sample selection

Histological samples were collected at diagnosis, before the start of systemic treatment. Tumor samples were reviewed by an expert pathologist, and the diagnosis of SCLC was confirmed histomorphologically by H&E staining and specific immunohistochemistry. Only samples with sufficient tumor tissue available were included in the analyses.

GEP analysis

Total RNA was extracted from two consecutive 10 µm thick formalin-fixed paraffin-embedded (FFPE) sections using the RNeasy FFPE kit (Qiagen); GEP was performed using the PanCancer IO360 panel (NanoString Technologies), as previously described.[22] The nCounter Advanced Analysis module V.2.0.134 software (NanoString Technologies) was used for differential expression analysis, and to discriminate cell types and pathways based on the expression of predefined genes.

Multiplex immunofluorescence

Multiplex immunofluorescence (mIF) was performed on sequential 4 µm thick FFPE tumor tissue sections using the Opal Polaris 7-Color Automated IHC Detection Kit (Akoya Biosciences) on the BOND-RX autostainer (Leica Microsystems). Two 9-color panels were used to characterize the subsets of tumor-infiltrating immune cells and the expression of transcription factors for ES-SCLC classification. More detailed information about methodology and antibodies is reported in online supplemental tables 1,2 respectively.

Multiplex slides were imaged using Mantra Quantitative Pathology Workstation V.2.0 (Akoya Biosciences) at ×20 magnification. The largest number of fields of view (FOV) per sample has been acquired, up to a maximum of 20 FOV/slide in large dimension tissue samples. Only areas containing tumor cells were included, and tissue samples with insufficient tumor areas or with high percentage of necrosis were excluded from the analyses. The inForm Image Analysis software (V.2.6, Akoya Biosciences) was used for analysis using representative multispectral images to train algorithms. Synaptophysin/chromogranin-A/NCAM staining was used in the tissue

J Immunother Cancer: first published as 10.1136/jitc-2024-008974 on 1 July 2024. Downloaded from http://jitc.bmj.com/ on December 31, 2024 by guest. Protected by copyright.

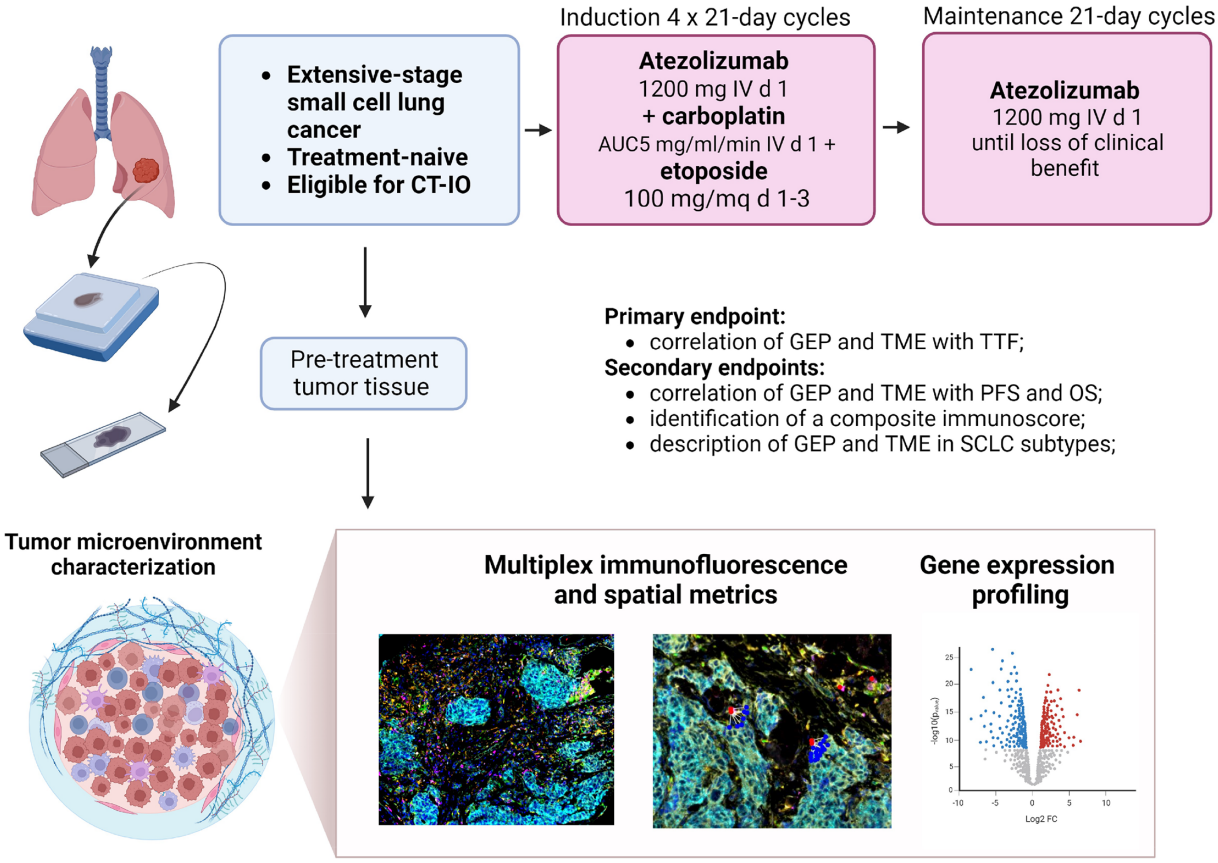

Figure 1 Study design. Created with biorender.com. AUC, area under the curve; d, day; CT-IO, chemoimmunotherapy; EP, gene expression profile; IV, intravenous; TTF, time-to-treatment failure.

segmentation step to differentiate infiltrating immune cells within the tumor areas and in the surrounding stroma. Individual cells were then segmented by nuclear counterstaining and colocalized cell surface or intracellular markers were used to determine cell phenotypes. Cell density data were calculated as the sum of the cells positive for a specific marker, divided by the total area analyzed from the same tissue slide. Cell density and cell percentage results refer to the total area analyzed (tumor plus stroma), the intratumoral area only or the peritumoral/stromal only, as indicated. Spatial metrics between cells within each tissue section were calculated using PhenoptrReports (add-ins for R Studio from Akoya Biosciences).[22]

SCLC subtypes scoring criteria

Transcription factor expression was recorded according to percentage of positive cells (1%–100%) and intensity of labeling (1=weak, 2=moderate, and 3=strong). A histoscore (H-score) was derived by multiplying the percentage of positivity by the intensity score, as previously described.[23] To define the dominant phenotype for cases expressing both ASCL1 and NEUROD1, the higher H-score defined the underlying SCLC subtype. Four subtypes of SCLC were identified on the basis of the protein expression of ASCL1 (SCLC-A), NEUROD1 (SCLC-N), POU2F3 (SCLC-P), and triple negative (SCLC-I) as previously performed by Baine *et al*.[24]

Activity and efficacy outcomes

TTF was defined as the time from treatment initiation to the earliest date of clinical/radiological progression requiring a change of treatment or death while PFS and OS as the time from treatment initiation to disease progression or death, and from diagnosis of ES-SCLC to death from any cause or last follow-up, respectively. Both response to treatment and disease progression were assessed using Response Evaluation Criteria In Solid Tumor .1.1. Patients who experienced a partial or complete response to treatment were classified as responders while those with stable disease or disease progression as best response to treatment were classified as non-responders.

Statistical methods

Sample size was estimated to test whether the TTF was heterogeneous at the high and low levels of the developed score, considered as a binary variable. Assuming a proportion of 50% of the total sample size at each score level, a total of 22 events would have provided 80% power to test an HR of 0.3 at a two-sided significance level of 0.05. Assuming a planned 2-year follow-up and a baseline event rate of 0.8 for the worst survival stratum, 20 patients would have been needed in each stratum to observe the required number of events. Patient demographics and clinical characteristics were described as median and IQR for continuous variables and as counts and percentages

J Immunother Cancer: first published as 10.1136/jitc-2024-008974 on 1 July 2024. Downloaded from http://jitc.bmj.com/ on December 31, 2024 by guest. Protected by copyright.

for categorical variables. Differential expression of the GEP and characterization of the immune TME were compared between the groups of interest using the non-parametric two-tailed Mann-Whitney test. Kaplan-Meier method was used to estimate the survival probabilities and median time was reported along with the corresponding 95% CI estimated using the Brookmeyer-Crowley method. To identify important predictors and build parsimonious models that balance predictive accuracy and model complexity, we proceeded as follows: from the original dataset of size n, we drew a sample with replacement of size n. Each marker in the bootstrap sample was categorized according to its derived median value and a least absolute shrinkage and selection operator (LASSO) Cox proportional hazards regression was fit to select the subset of markers that minimized model error. A 10-fold cross-validation was used to identify the shrinkage parameter λ that yielded the model with the lowest error for the Harrell's concordance measure.

This process was repeated 1000 times and the 30% most selected markers were used as candidate predictors in a Cox proportional hazards regression model. A backward selection procedure with the Bayesian information criterion was applied for retaining the number of authentic variables in the final model. The final model was validated for calibration and discrimination using bootstrap, and parameter estimates were shrunk to reduce overfitting.

Results are presented in terms of HR together with 95% CI. The Grambsch and Therneau test statistic did not indicate a departure from the assumption of proportional hazards.

Patients were stratified into high-risk and low-risk groups based on their predicted risk of TF derived from the final multiple Cox model. The linear predictor was calculated for each patient as the sum of the product of each marker's coefficient and the corresponding value of that marker for the patient. The linear predictor median value, calculated on the data, was chosen as the cut-off point.

Using LASSO regression, results were not adjusted for multiple comparisons. Cross-validation was used to tune the regularization parameter and bootstrap to evaluate the robustness of variable selection and reduce overfitting. As a measure of predictive accuracy, Harrell's C-index was provided.

All statistical tests used a two-sided 5% significance level. Statistical analyses were performed using GraphPad Prism software (V.8.0), IBM SPSS Statistics (V.28) and RStudio (RStudio: Integrated Development for R, RStudio, Boston, Massachusetts, USA).

RESULTS

Patient characteristics and treatment outcome

At cut-off date (April 30, 2023), 42 ES-SCLC patients were included in the study, whose characteristics are summarized in table 1.

Table 1 Patients' characteristics

Variable	N (%)	
Number of cases	42	(100, 0)
Age (years), median (IQR)	69.9	(57.5–73.3)
Gender		
Male	25	(59.5)
Female	17	(40.5)
Comorbidity		
Yes	29	(69.0)
No	13	(31.0)
Recurrent		
Yes	4	(9.5)
No	38	(90.5)
Smoking status		
Never smokers	3	(7.1)
Former smokers	19	(45.2)
Smokers	20	(47.6)
Packs-Years, median (IQR)	40	(30–53.5)
Professional exposure		
Yes	8	(19.0)
No	34	(80.9)
Histology		
SCLC	42	(100.0)
Mixed SCLC	0	(0.0)
Ki67, median (IQR)	82,5	(77.5–90.0)
Stage at diagnosis		
IIIC	1	(2.4)
IVA	4	(9.5)
IVB	37	(88.1)
Tissue samples		
Primary tumor and regional nodes	28	(66.7)
Metastasis	14	(33.3)
ECOG PS		
0–1	34	(81.0)
≥2	8	(9.0)
Symptoms at diagnosis		
Present	29	(69.0)
Absent	13	(31.0)
Charlson Comorbidity Index		
6–7	12	(28.6)
>7	30	(71.4)
Number of metastatic sites at diagnosis		
<3	27	(64.3)
≥3	15	(35.7)
Brain metastasis at diagnosis		
Present	12	(28.6.)
Absent	30	(71.4)

Continued

J Immunother Cancer: first published as 10.1136/jitc-2024-008974 on 1 July 2024. Downloaded from http://jitc.bmj.com/ on December 31, 2024 by guest. Protected by copyright.

Table 1 Continued

Variable	N (%)	
Liver metastasis at diagnosis		
Present	18	(42.9)
Absent	24	(57.1)
Bone metastasis at diagnosis		
Present	13	(31.0)
Absent	29	(69.0)
Steroid therapy at treatment start		
No	23	(54.7)
Yes	19	(45.2)
Antibiotic therapy at treatment start		
No	37	(88.1)
Yes	5	(10.2)

ECOG PS, Eastern Cooperative Oncology Group performance status; N, number; SCLC, small-cell lung cancer.

25 (59.9%) were males, 49 (92.8%) were former or current smokers; median age was 69.9 years (IQR 57.5–73.3). 41 patients (97.6%) had stage IV disease at diagnosis. Samples included primary tumors and regional lymph nodes in 32 (76.2%) cases, and metastases in 10 (23.8%) cases. The overall response rate was 66% (95% CI 51.9% to 81.5%). After a median follow-up of 23.5 months (IQR 10.5–NE), the estimated median TTF, PFS and OS of the study population were 5.3 months (95% CI 4.4 to 7.2), 5.3 months (95% CI 4.4 to 6.9), and 7.8 months (95% CI 6.5 to 13.8), respectively. There were 36 (61.9%) responders, and 13 (33.3%) non-responders; 3 cases were not radiologically evaluated.

At univariate analysis, a longer TTF was observed in females compared with males (p=0.032), in patients with fewer than three metastatic sites at diagnosis (p<0.001) and in patients not receiving steroid therapy at the start of treatment (p=0.007). The number of metastatic sites (HR 4.440, 95% CI 1.043 to 18.910) and steroid therapy (HR 0.204, 95% CI 0.0543 to 0.769) were confirmed to be independently associated with TTF at multivariate analysis (online supplemental table 3).

Clinical features impacting on PFS were gender (p=0.014) and the number of metastatic sites at diagnosis (p=0.010). A trend toward better a PFS was observed in patients not receiving steroid treatment at diagnosis (p=0.061). Multivariate analysis confirmed gender (HR 0.251, 95% CI 0.0744 to 0.850) and steroid treatment as factors independently correlated with PFS (HR 0.237; 95% CI 0.0691 to 0.813) (online supplemental table 4).

In terms of OS, fewer than three metastatic sites at diagnosis (p<0.001), PS ECOG less than 2 at diagnosis (p=0.009) and absence of steroid therapy at the start of treatment (p=0.011), were associated with better outcomes on univariate analysis. There was also a trend toward a longer OS in responders (p=0.072). Multivariate analysis confirmed PS (HR 0.151, 95% CI 0.022 to 1.027) and the number of metastatic sites at diagnosis as independent prognostic factors (HR 6.981, 95% CI 1.685 to 28.920) (online supplemental table 5).

When we assessed the impact of clinical factors at the multivariate analysis including predictive biomarkers, the significant impact of gender (p=0.041) and steroid therapy (p=0.007) on PFS and the number of metastatic sites on OS (p=0.047) have been confirmed (online supplemental table 6).

Immune/cancer-related pathway activation and correlation with outcome

After RNA extraction, 39 (93%) samples passed the quality controls and were analyzed for GEP. The multiple Cox regression model showed a significant reduction in the risk of TF in those tumors with higher expression of exhausted CD8-related genes (HR 0.34, 95% CI 0.15 to 0.75, p=0.0072) and higher levels of CD79A (HR 0.29, 95% CI 0.12 to 0.67, p=0.0038) and TNFRSF25 (HR 0.41, 95% CI 0.18 to 0.91, p=0.0292) genes while a similar but non-significant trend was seen for mTOR (HR 0.50, 95% CI 0.22 to 1.09, p=0.0827) (figure 2).

Similarly, higher expression of exhausted CD8-related genes (HR 0.20, 95% CI 0.06 to 0.61, p=0.0050) was an independent positive predictor of PFS. Higher gene expression of mTOR (HR 0.25, 95% CI 0.10 to 0.61, p=0.0023), CD47 (HR 0.18, 95% CI 0.07 to 0.48, p=0.0006) and PFKFB3 (HR 0.41, 95% CI 0.18 to 0.91, p=0.00297) was significantly associated with a longer PFS (figure 2).

Finally, overexpression of exhausted CD8-related genes (HR 0.30, 95% CI 0.14 to 0.66, p=0.0026) and of HEY1 gene (HR 0.33, 95% CI 0.16 to 0.78, p=0.0104) were independently associated with a decreased risk of death, whereas hyperexpression of EIF5AL1 gene (HR 4.13, 95% CI 1.72 to 9.92, p=0.0015) showed a negative prognostic value (figure 2).

Immune microenvironment characterization and correlation with outcome

Sufficient tumor tissue for mIF was available for 39 (93%) cases. More than 80% of tumor cells were negative for HLA-class I expression (online supplemental figure 1A) in most patients. Lymphocytes were mainly composed of CD8+cells and were preferentially detected in the peritumoral/stromal regions (online supplemental figure 1B); overall, the immune infiltrate was mainly composed of macrophages, in particular M2-polarized CD163+cells, both within the tumor regions and in the peritumoral/stromal areas (online supplemental figure 1C).

In multivariate analysis, a higher CD8+T lymphocyte infiltration in the total area (HR 0.30, 95% CI 0.13 to 0.69, p=0.0049) and a higher CD4+T lymphocyte density in the stroma (HR 0.23, 95% CI 0.10 to 0.53, p=0.0005), were correlated with a lower risk of TF. Conversely, a higher CD68+macrophage/CD8+T lymphocyte ratio within the tumor regions correlated with a worse outcome in terms of TTF (HR 4.00, 95% CI 1.64 to 9.77, p=0.0023).

J Immunother Cancer: first published as 10.1136/jitc-2024-008974 on 1 July 2024. Downloaded from http://jitc.bmj.com/ on December 31, 2024 by guest. Protected by copyright.

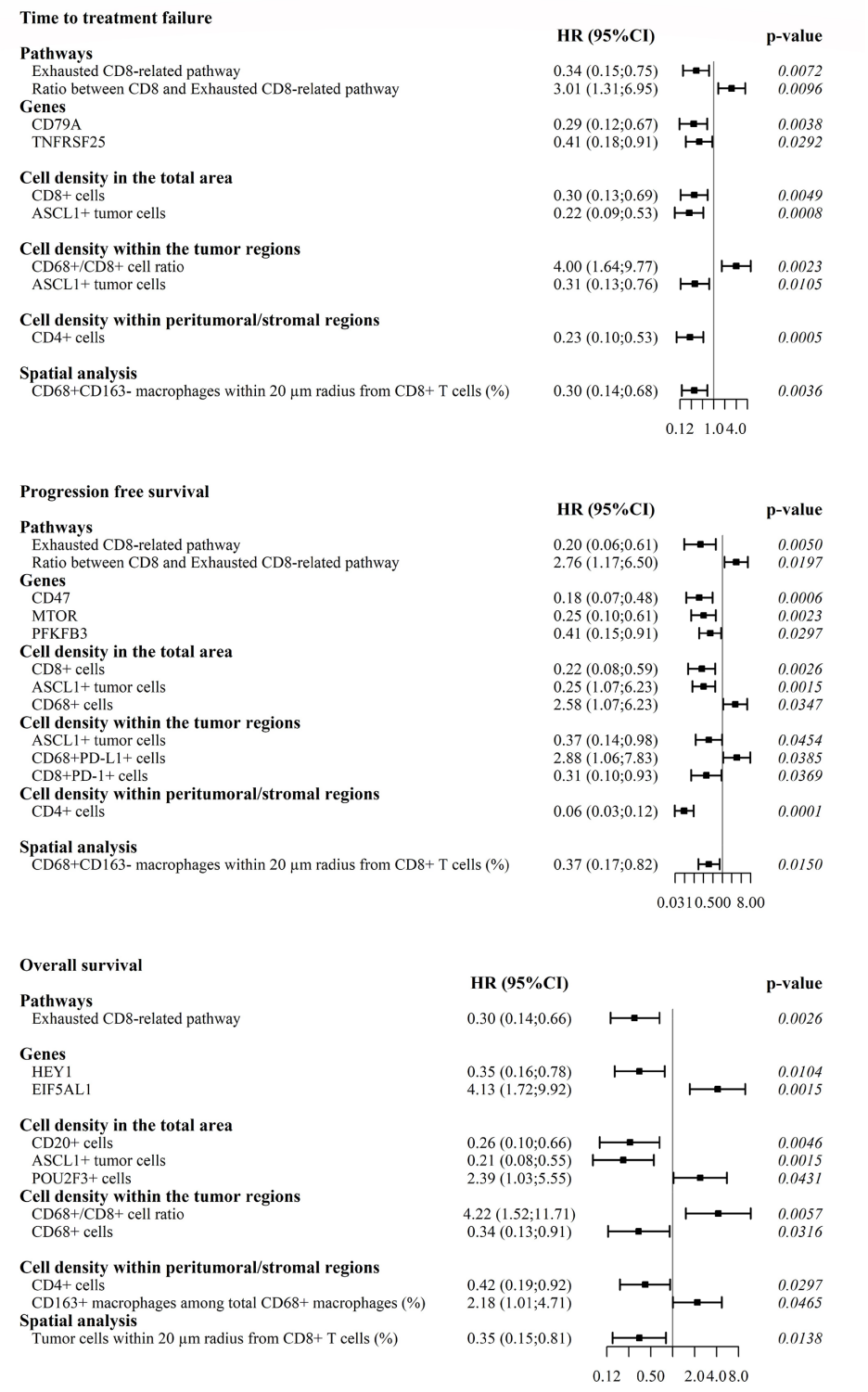

Figure 2 Forest plots of multivariate analyses illustrating independent factors associated with time-to-treatment failure (TTF), progression-free survival (PFS) and overall survival (OS) for extensive-stage small-cell lung cancer (ES-SCLC). The horizontal axes represent the OR with reference line, ORs (cube), and 95% CI (whiskers). ASCL1; achaete-scute family bHLH transcription factor; POU2F3, POU class 2 Homeobox 3; PD-L1, programmed death-ligand 1; PD-1, programmed cell death protein 1; HEY1, Hairy/enhancer-of-split related with YRPW motif protein 1; EIF5AL1; Eukaryotic Translation Initiation Factor 5A Like 1.

The analysis of the spatial distribution of cells within the TME showed that a higher percentage of CD68+CD163– M1-like macrophages close to CD8+T lymphocytes (within a 20 µm radius) correlated with a better TTF (HR 0.30, 95% CI 0.14 to 0.68 p=0.0036) (figure 2).

When we investigated the potential impact of TME composition and cell-to-cell interactions on PFS, an independent positive predictive role was confirmed for a higher density of CD8+T lymphocyte in the total area (HR 0.22, 95% CI 0.08 to 0.50, p=0.0026), PD-1-expressing

J Immunother Cancer: first published as 10.1136/jitc-2024-008974 on 1 July 2024. Downloaded from http://jitc.bmj.com/ on December 31, 2024 by guest. Protected by copyright.

CD8+T cells in the tumor (HR 0.31, 95% CI 0.10 to 0.93, p=0.0369) and CD4+T lymphocytes within the stroma (HR 0.06, 95% CI 0.03 to 0.12, p=0.0001), as well as a higher percentage of CD68+CD163− M1-like macrophages close to CD8+T lymphocytes (HR 0.37, 95% CI 0.17 to 0.82, p=0.0150). On the contrary, an increased risk of disease progression was observed in patients with higher density of CD68+macrophages in the total area (HR 2.58, 95% CI 1.07 to 6.23, p=0.0347) and higher PD-L1 expression on macrophages within the tumor regions (HR 2.88, 95% CI 1.06 to 7.83, p=0.0385) (figure 2).

Although OS may be influenced by clinical factors and postprogression therapies, we investigated the pure impact of the microenvironment on patient prognosis. A higher infiltration of CD20+B lymphocytes in the total area (HR 0.26, 95% CI 0.10 to 0.66, p=0.0046) and of CD4+T lymphocytes in the stroma (HR 0.42, 95% CI 0.19 to 0.92, p=0.0297) was associated with longer survival while a higher risk of death correlated with an increased CD68+macrophage/CD8+T lymphocyte ratio within the tumor compartment (HR 4.22, 95% CI 1.52 to 11.71, p=0.0057) (figure 2).

Transcriptomic profiling and immune cell composition in SCLC subtypes, and association with outcomes

Four subtypes of SCLC were identified by mIF according to the differential expression of the transcription factors ASCL1, NEUROD1 and POU2F3 (online supplemental figure 2A,B). Notably, in some patients coexpression of different transcription factors, particularly ASCL1 and NEUROD1, was present in various tumor areas suggesting intratumor plasticity with multiple coexisting subtypes within a single tumor (online supplemental figure 2C).

SCLC tumors were not evenly distributed among the four subtypes, with the SCLC-A subtype (36%) being the most common followed by SCLC-I (33%), SCLC-N (19%), and SCLC-P (12%). In our cohort, patients with SCLC-A tumors achieved longer survival while SCLC-N had a dismal prognosis (figure 3A).

We found differences among the four SCLC subtypes with regard to signaling pathways and immune markers. Indeed, with the exception of macrophages, all the other immune populations were less represented in SCLC-N tumors compared with the other subtypes (figure 3B). Moreover, FoxP3+/CD8+and CD68+/CD8+cell ratios were higher in SCLC-N (figure 3C). Within the tumor region of the SCLC-A subtype, we detected an increased percentage of CD8+T cells within a 20 µm radius from CD68+CD163− M1-like macrophages, whereas SCLC-N showed the highest percentage of CD8+lymphocytes in close proximity to M2-like macrophages (figure 3D,F). Finally, SCLC-A showed more PD-1+CD8+ T cells close to PD-L1+macrophages and tumor cells as compared with the other SCLC subtypes (figure 3E,F).

In addition, data obtained by gene expression analysis stratifying patients according to the H-score matched with the characteristics of each SCLC subtype described in literature, as we found that MYC gene was upregulated in SCLC-N subtypes as compared with SCLC-A (log2 fold-change=3.88, adj. p-≤0.001) and SCLC-I (log2 fold-change=2.82, adj. p=0.03). Moreover, genes associated with Notch, Hedgehog and Wnt signaling pathways were upregulated in SCLC-P and SCLC-I as compared with SCLC-N and SCLC-A (online supplemental figure 3A), in line with the observation that their activation promotes the non-neuroendocrine SCLC fate.[25]

Furthermore, we found that SCLC-I tumors had an upregulation of genes associated with T-cells and B-cells (online supplemental figure 3B), and genes involved in cytokine and chemokine signaling, lymphoid compartment and tumor-inflammation signature (online supplemental figure 3C). Accordingly, a greater expression of several immune-related genes has been observed in non-neuroendocrine tumors, and in particular in the SCLC-I inflamed-subtype.[20 26]

Multiple Cox regression model disclosed that a higher tumor expression of ASCL1 was associated with a lower risk of TF (HR 0.2231, 95% CI 0.1309 to 0.7653, p=0.0105008), disease progression (HR 0.3725, 95% CI 0.141 to 0.9859, p=0.0015454) and death (HR 0.21, 95% CI 0.08 to 0.55, p=0.0015) while a higher risk of death correlated with an increased POU2F3 expression (HR 2.39, 95% CI 1.03 to 5.55, p=0.0431) (figure 2).

A combined transcriptional, phenotypical and topological score allows to stratify patient outcome

We investigated the overall impact of activated pathways, immune cell contexture and transcription factor expression on TTF, PFS and OS in multivariate analysis.

When the three features were assessed together, a lower risk of TF was observed in the presence of a higher activation of the exhausted CD8+T lymphocyte-related pathway (HR 0.20, 95% CI 0.07 to 0.45, p=0.0026), more abundant CD20+B lymphocytes in the total area (HR 0.30, 95% CI 0.11 to 0.83, p=0.0206), and an augmented ASCL1 expression in tumor cells (HR 0.15, 95% CI 0.05 to 0.46, p=0.0011). Conversely, an increased presence of CD163+macrophages close to (20 µm) tumor cells correlated with a higher risk of TF (HR 2.80, 95% CI 1.00 to 7.82, p=0.0491) (figure 4).

Overexpression of exhausted CD8+T lymphocyte-related genes (HR 0.21, 95% CI 0.08 to 0.57, p=0.0020) and a higher ASCL1 expression in tumor cells (HR 0.18, 95% CI 0.07 to 0.50, p=0.0011) were also associated with a lower risk of disease progression (figure 4).

A higher tumor expression of POU2F3 (HR 3.37, 95% CI 1.06 to 10.76, p=0.0402) was correlated with a higher risk of death while more infiltration of CD20+B lymphocytes in the total area (HR 0.31, 95% CI 0.11 to 0.89 p=0.0295), an increased tumor expression of ASCL1 (HR 0.16, 95% CI 0.05 to 0.55 p=0.0034) and a higher presence of CD8+close to CD4+T lymphocytes (HR 0.26, 95% CI 0.07 to 0.90 p=0.0340), were associated with a lower risk (figure 4).

At the multivariate analysis including both biological features and clinical characteristics of the patients, we

J Immunother Cancer: first published as 10.1136/jitc-2024-008974 on 1 July 2024. Downloaded from http://jitc.bmj.com/ on December 31, 2024 by guest. Protected by copyright.

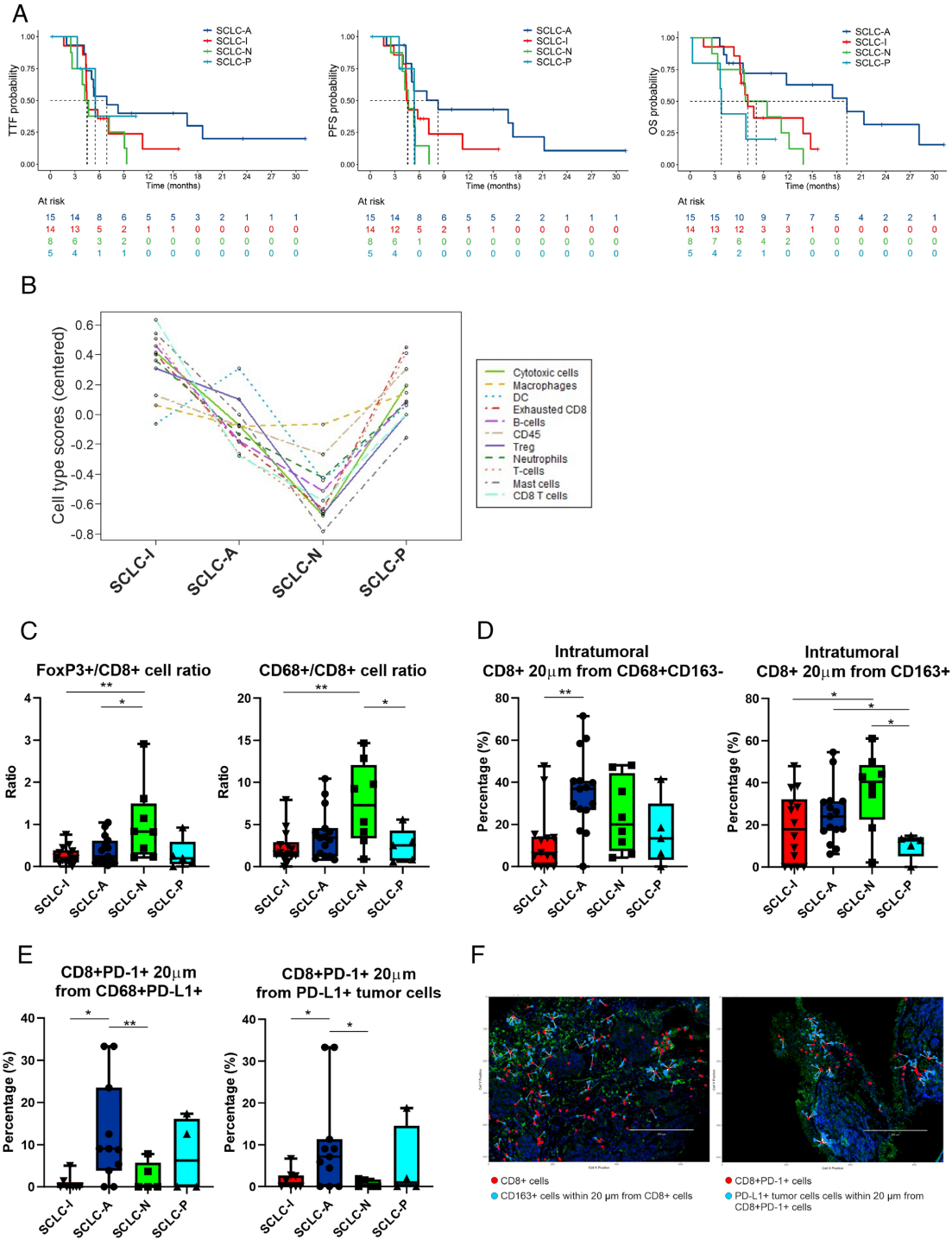

Figure 3 Small-cell lung cancer (SCLC) subtypes have different tumor immune microenvironmen (TME) composition. (A) Kaplan-Meier curves for time-to-treatment failure (TTF), progression-free survival (PFS) and overall survival (OS) according to the SCLC classification based on ASCL1, NEUROD1 and POU2F3 transcription factors expression. (B,C) Immune cells infiltrating the TME of SCLC subtypes. (D,E) Spatial metrics analysis in SCLC subtypes. (F) Representative images of spatial metrics analysis performed. In the left picture, CD163+macrophages within a 20 µm radius from CD8+cells are represented while the picture on the right shows PD-L1+tumor cells within a 20 µm radius from CD8+PD-1+ cells

confirmed the correlation with TTF, PFS and OS of the identified transcriptional, phenotypical and topological scores adjusted for clinical factors, with the exception of CD163+macrophages close to (20 µm) tumor cells on TTF analysis (online supplemental table 6).

In conclusion, we categorized patient population into a high-risk and a low-risk group according to the median of a combined score that included the expression of exhausted CD8+T lymphocyte-related genes, the infiltration of CD20+B lymphocytes in the total area, the

J Immunother Cancer: first published as 10.1136/jitc-2024-008974 on 1 July 2024. Downloaded from http://jitc.bmj.com/ on December 31, 2024 by guest. Protected by copyright.

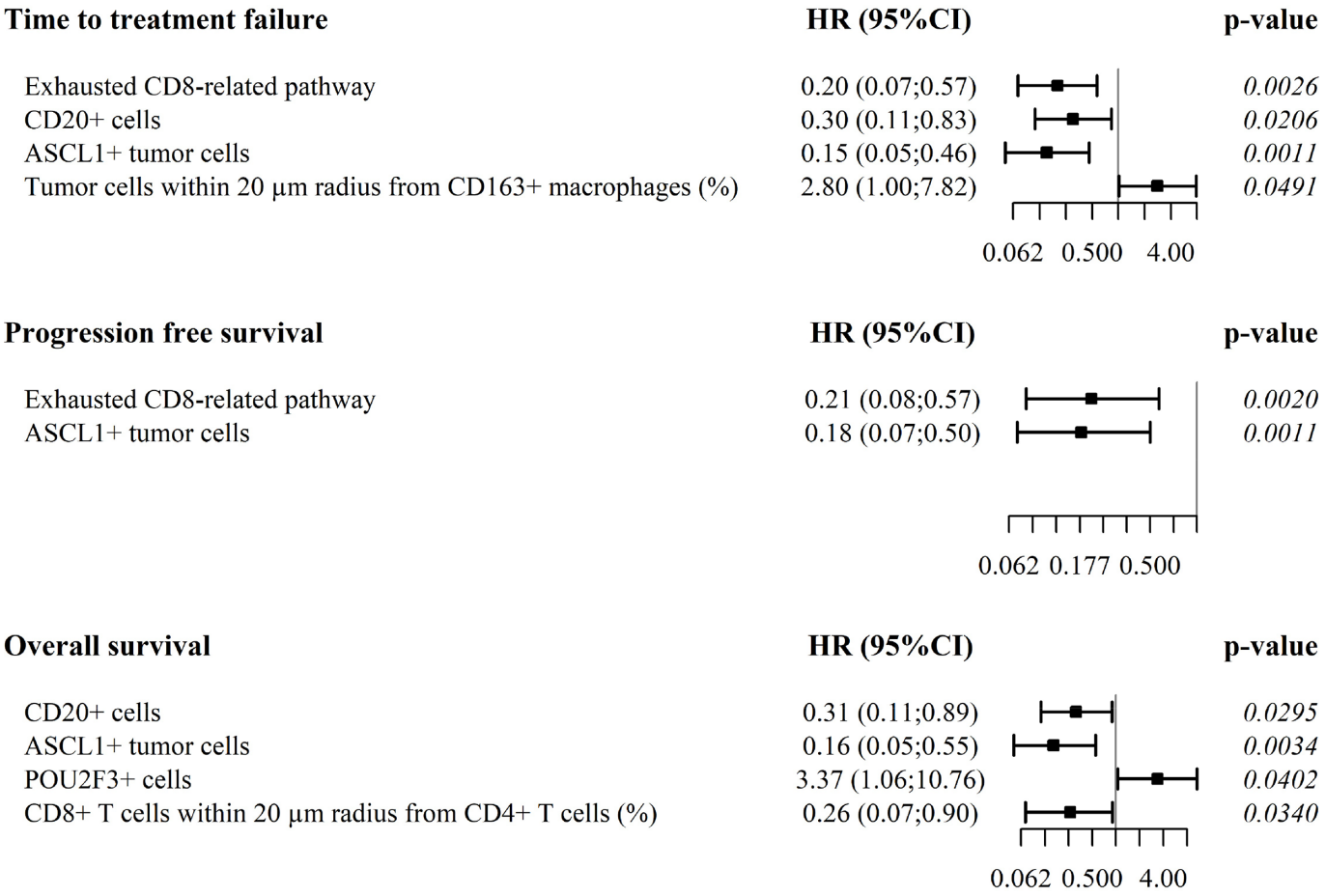

Figure 4 Forest plots of multivariate analyses illustrating the overall impact of activated pathways, immune cell contextures and transcription factors expression on time-to-treatment failure (TTF), progression-free survival (PFS) and overall survival (OS) for extensive-stage small-cell lung cancer (ES-SCLC). The horizontal axes represent the OR with reference line, ORs (cube), and 95% CI (whiskers).

expression of ASCL1 in tumor cells and the presence of CD163+macrophages close to tumor cells. Median TTF, PFS and OS were 9.0, 6.2 and 17.5 months in the low-risk group and 4.4, 4.4 and 6.6 months in the high-risk group, respectively (figure 5A). The estimated HRs of the high-risk group were 4.15 (95% CI 1.77 to 9.71), 3.16 (95% CI 1.38 to 7.24), and 3.64 (95% CI 1.47 to 9.01) for TTF, PFS, and OS, respectively. The combined score showed higher performance in the risk stratification compared with the single variables (figure 5B).

DISCUSSION

Despite advances in the treatment of SCLC with the advent of ICIs in combination with chemotherapy, the stratification of patient outcome remains an urgent unmet medical need. Tissue and other circulating biomarkers, as well as clinical features, have failed to demonstrate a strong predictive role. Recently, however, new perspectives have been opened by the recent identification of four transcriptionally distinct subtypes of SCLC with different therapeutic vulnerabilities.[19]

In this work, we performed a biomarkers analysis on tumor tissue achieved during the diagnostic pathway of patients before the treatment started. Survival outcomes are comparable to previous real-world data and negatively influenced by the inclusion of patients with poor performance status, active brain metastasis, comorbidity and with a high disease burden, generally excluded from large randomized clinical trial.[27–30]

In line with the literature data, the low expression of HLA-I as well as the limited number of immune cells, reflects an immune-cold TME.[31]

In our cohort, the distribution of SCLC subtypes is in line with previously reported data.[20 24] We observed a different composition of the immune TME among the four subtypes, with the SCLC-N being the less infiltrated as already described.[32] We also found that ASCL1 expression by tumor cells is an independent positive prognostic and predictive factor. While this appears quite in contrast with previous evidence, some considerations have to be done. We performed the subtype analysis at a protein level, using a validated method and antibodies tested by Baine *et al* in the comprehensive analysis of immunohistochemical SCLC subtypes,[24] which seems more reliable for clinical practice use. However, a huge biological complexity,

J Immunother Cancer: first published as 10.1136/jitc-2024-008974 on 1 July 2024. Downloaded from http://jitc.bmj.com/ on December 31, 2024 by guest. Protected by copyright.

A

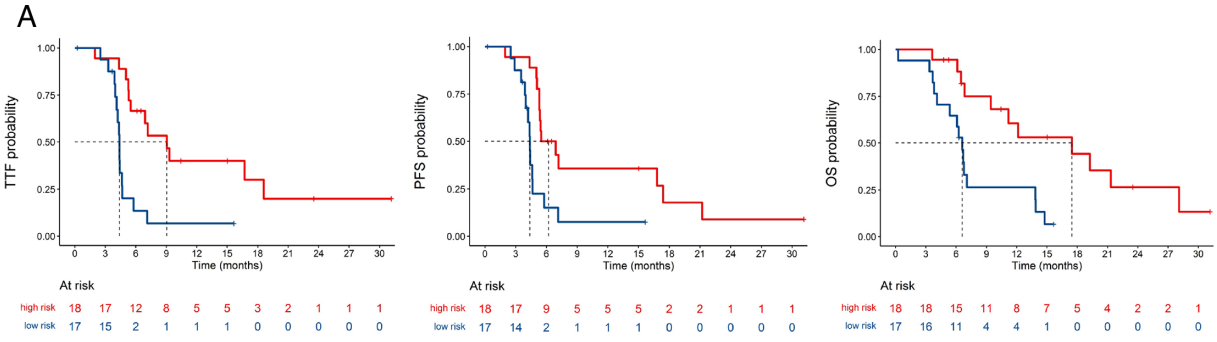

B

	Harrell's C-index		
	TTF	PFS	OS
Score	**0.80**	**0.72**	**0.80**
Exhausted CD8-related pathway	0.64	0.63	
CD20+ cells	0.59		0.63
ASCL1+ tumor cells	0.64	0.64	0.63
Tumor cells within 20 µm radius from CD163+ macrophages (%)	0.61		
POU2F3+ cells			0.55
CD8+ T cells within 20 µm radius from CD4+ T cells (%)			0.63

Figure 5 Stratification of patient risk based on the identified combined score. (A) Kaplan-Meier curves for time-to-treatment failure (TTF), progression-free survival (PFS) and overall survival (OS) according to the identified combined score. (B) The performance (Harrell's C-index) of the combined score as compared with the single variables.

due to plasticity and subtypes interconversion, has been identified in SCLC, in particular for SCLC-A and SCLC-N.[32] The more recent analysis of long-term survivors from IMpower133 trial showed that a higher proportion of long-term survivors in both arms had the SCLC-I subtype.[33] This led to the identification, through non-negative matrix factorization, of two inflamed subsets with differential neuroendocrine phenotypes: the neuroendocrine SCLC-I-NE subset and the non-neuroendocrine SCLC-I-nonNE subset.[34] Interestingly, the SCLC-I-NE subset could express the transcription factors ASCL1 and obtains a significant benefit from the addiction of atezolizumab. Moreover, the authors suggest the tumor-associated macrophage (TAM)/T-effector ratio is associated with outcome in the immune-enrich subsets. In line with these findings, in our case series, the SCLC-A subtype is characterized by the highest percentage of PD-1+T cells in close proximity to PD-L1-positive macrophages and tumor cells. These results are in line with observations in metastatic melanoma where the proximity between PD-1 and PD-L1 correlates with response to ICI,[35] and suggests the importance of an exhausted TME in the response to immunotherapy in ES-SCLC. Accordingly, we showed that patients with high expression of the exhausted CD8-related gene signature have a better outcome. Chronic antigen exposure and T cell receptor stimulation are required for exhaustion programs in T cells.[36] Recently, a paradigm shift is emerging in the comprehension of T cell exhaustion in cancer. Single-cell transcriptomic and epigenetic profiling have led to the identification of two distinct subtypes of "dysfunctional" T cells in a continuum spectrum: "progenitor" and "terminally" exhausted cells.[37] While "progenitor" exhausted T cells exhibit poor cytotoxicity but are long-lived with stem-like properties, "terminally" exhausted T cells have increased cytotoxicity but are short-lived.[38] In melanoma patients, ICIs induce the differentiation of stem-like "progenitor" exhausted T cells into cytotoxic "terminally" exhausted T cells to temporarily control the tumor, and the presence of "progenitor" exhausted CD8+T cells correlates with long-term responses to ICIs.[39] An increase in "progenitor" exhausted T cells has been also identified in NSCLC patients who responded to PD-L1-based therapies.[40] Therefore, there is a strong rationale to further investigate the role of this subset in SCLC patients to confirm its predictive role. To note, a biological change in the tumor biology and infiltrate could occur during the course of therapy, highlighting the dynamic heterogeneity of this disease. However, repeated tissue biopsies to investigate the plasticity of the disease are not feasible in the clinical practice and the identification of predictive biomarkers is needed a priori for treatment-naïve patients.

TAMs are the most abundant cell type in the TME of our patient cohort, consistent with previous findings in surgical specimens of limited-stage disease.[41] M2-like macrophages are associated with the worst outcomes in a heterogeneous SCLC patient population.[42] Consistently, we found a negative association between higher rates of

J Immunother Cancer: first published as 10.1136/jitc-2024-008974 on 1 July 2024. Downloaded from http://jitc.bmj.com/ on December 31, 2024 by guest. Protected by copyright.

macrophage vs CD8+cells infiltration in the tumor region, and treatment outcome.

The first added value of our study is offered by the assessment of the immune cell infiltrate not only in a merely quantitative manner, but also through a spatial metric analysis that allows to capture the role and interaction of cell subtypes. Indeed, the proximity between CD8+T cells and M1-like macrophages is associated with a better treatment outcome, likely reflecting an active antitumor immunological response or a direct role of macrophages in antitumor defense on interaction with cytotoxic T cells, as already reported in colon cancer.[43] Conversely, the proximity between tumor cells and CD163+M2 like macrophages correlates with a higher risk of TF. Indeed, M2-polarized macrophages have been shown to express and release molecules that directly promote cancer cell proliferation.[44]

The close association between tumor and immune cells within the TME leads to competition for nutrients. High expression of proteins involved in glycolysis has been reported to be associated with poor prognosis in lung cancer.[45] The proliferation and survival of most cancer cells are more dependent on aerobic glycolysis, whereas T cells mainly depend on the oxidative phosphorylation pathway.[46] However, aerobic glycolysis is required for T cell activation, function, and differentiation.[47] Moreover, proinflammatory M1-like macrophages are dependent on glycolysis while immunosuppressive M2-like TAMs are dependent on the tricarboxylic acid cycle and fatty acid oxidation, and therefore, use the Krebs cycle instead of glycolysis.[48] Since the interaction between immune checkpoints and their ligands regulates the metabolism of tumor and immune cells,[49] ICIs could restore the extracellular glucose concentration in the TME and increase the glycolytic activity of T cells.[50] Moreover, the metabolic profile of tumor cells may be related to the likelihood of response to anti-PD-1 immunotherapy, as ICIs are most effective in highly glycolytic tumors.[51] In this scenario, we found that patients with a high expression of genes involved in glycolysis and in the promotion of the Warburg effect (mTOR, PFKFB3)[52 53] have a lower risk of progression. Under PD1/PDL1-targeted immunotherapy, mTOR is also required to efficiently generate effector-like transitory T cells during chronic viral infection,[54] supporting the use of metabolic modulators, especially those that target oxidative metabolism, to sustain immunotherapeutic response. However, this hypothesis is purely speculative since bulk mRNA analysis is unable to distinguish the type of cell where the expression is evident. Further investigation is needed to confirm the predictive role of glycolysis in SCLC under the ICIs effect.

The second added value of this work relies on the integration of different biomarkers into a prognostic score. We used GEP, cell phenotype analysis and the measurement of spatial cell distribution to define a combined prognostic factor, which encompasses the expression of exhausted CD8+-related genes, the density of CD20+B cells, the density of ASCL1+tumor cells and the proximity between tumor cells and M2-like macrophages, ultimately capable of stratifying ES-SCLC patients into high-risk and low-risk groups. Notably, although these variables were independent predictors of TF, the combined score showed good performance not only for TTF but also for PFS and OS.

We are aware that the main limitations of this study are its exploratory nature and the small sample size, which requires validation of the identified combined score in a larger patient cohort. The detection of the dynamic tumor heterogeneity over time is not within the aims of the present study, thus representing a possible limitation. However, an exploratory prospective translational study of our group is ongoing in order to identify circulating biomarkers predictive of treatment outcome, potentially useful for detecting early resistance markers during treatment, and finally showing intratumor heterogeneity and plasticity over time under treatment pressure.[55 56] Nonetheless, our data provide guidance for the introduction of new stratification biomarkers in future clinical trials and in the testing of new combination immune-based treatments, to increase patient benefit.

Author affiliations
[1]Immunology and Molecular Oncology Diagnostics, Istituto Oncologico Veneto IOV-IRCCS, Padova, Italy
[2]Department of Medical Oncology, Santa Chiara Hospital, Trento, Italy
[3]Clinical Trials and Biostatistics, Istituto Oncologico Veneto IOV-IRCCS, Padova, Italy
[4]Medical Oncology 3, Istituto Oncologico Veneto IOV-IRCCS, Castelfranco Veneto, Italy
[5]Department of Medical Oncology, AULSS 3 Serenissima, Venezia, Italy
[6]Pathology Unit, Istituto Oncologico Veneto IOV-IRCCS, Padova, Italy
[7]Department of Surgery, Oncology and Gastroenterology, University of Padova, Padova, Italy
[8]Medical Oncology 2, Istituto Oncologico Veneto IOV-IRCCS, Padova, Italy
[9]Department of CardioThoracic Vascular Sciences and Public Health, Università degli Studi di Padova, Padova, Italy

Contributors Conceptualization: GP, AR, and AT; Data curation: AT, ML, PDB, AR, AP, and MVR; Funding acquisition: GP, VG, and AR; Methodology: PDB, AT, GP, LB, and SF; Project administration: GP, AR, FC, and AS; Resources: GP, VG, AR, and PDB; Supervision: GP, VG, AR, and LB; Roles/Writing–original draft: AT, ML, MVR, and SF; Writing–review and editing: all authors; Guarantor: AR, GP.

Funding This work was unconditionally supported by Roche (ML43257) and DOR by the Department of Surgery, Oncology and Gastroenterology (DiSCOG), University of Padova.

Competing interests GP reports Advisory Boards/Honoraria/Speakers' fee/Consultant by Amgen, AstraZeneca, BMS, Eli Lilly, Jansenn, MSD, Novartis, Pfizer, Roche, and unconditioned research support by AstraZeneca, Roche, MSD. VG reports personal fees for advisory board membership for AstraZeneca, Daiichi Sankyo, Eisai, Eli Lilly, Exact Sciences, Gilead, Merck Serono, MSD, Novartis, Pfizer, Olema Oncology, Pierre Fabre; personal fees as an invited speaker for AstraZeneca, Daiichi Sankyo, Eli Lilly, Exact Sciences, Gilead, GSK, Novartis, Roche and Zentiva; personal fees for expert testimony for Eli Lilly.

Patient consent for publication Consent obtained directly from patient(s).

Ethics approval This study involves human participants and was approved by Ethical Committee of Istituto Oncologico Veneto IRCCS Padova, Italy, Participants gave informed consent to participate in the study before taking part.

Provenance and peer review Not commissioned; externally peer reviewed.

Data availability statement All data relevant to the study are included in the article or uploaded as online supplemental information.

Supplemental material This content has been supplied by the author(s). It has not been vetted by BMJ Publishing Group Limited (BMJ) and may not have been

J Immunother Cancer: first published as 10.1136/jitc-2024-008974 on 1 July 2024. Downloaded from http://jitc.bmj.com/ on December 31, 2024 by guest. Protected by copyright.

peer-reviewed. Any opinions or recommendations discussed are solely those of the author(s) and are not endorsed by BMJ. BMJ disclaims all liability and responsibility arising from any reliance placed on the content. Where the content includes any translated material, BMJ does not warrant the accuracy and reliability of the translations (including but not limited to local regulations, clinical guidelines, terminology, drug names and drug dosages), and is not responsible for any error and/or omissions arising from translation and adaptation or otherwise.

Open access This is an open access article distributed in accordance with the Creative Commons Attribution Non Commercial (CC BY-NC 4.0) license, which permits others to distribute, remix, adapt, build upon this work non-commercially, and license their derivative works on different terms, provided the original work is properly cited, appropriate credit is given, any changes made indicated, and the use is non-commercial. See http://creativecommons.org/licenses/by-nc/4.0/.

ORCID iDs
Laura Bonanno http://orcid.org/0000-0001-5218-4970
Giulia Pasello http://orcid.org/0000-0002-8741-6038

REFERENCES

1 Howlade N, Noone AM, Krapcho M, *et al*. National Cancer Institute SEER cancer Statistics review 1975-2013 National Cancer Institute. In: *SEER Cancer Statistics Review 1975-2013*. Bethesda, MD, 2016: 1992–2013. Available: http//seer.cancer.gov/csr/1975_2013/, based Novemb. 2015
2 Micke P, Faldum A, Metz T, *et al*. Staging small cell lung cancer: veterans administration lung study group versus International Association for the study of lung cancer - what limits limited disease *Lung Cancer* 2002;37:271–6.
3 Mascaux C, Paesmans M, Berghmans T, *et al*. A systematic review of the role of etoposide and cisplatin in the chemotherapy of small cell lung cancer with methodology assessment and Meta- analysis. *Lung Cancer* 2000;30:23–36.
4 Paz-Ares L, Dvorkin M, Chen Y, *et al*. Durvalumab plus platinum–etoposide versus platinum–etoposide in first-line treatment of extensive-stage small-cell lung cancer (CASPIAN): a randomised, controlled, open-label, phase 3 trial. *Lancet* 2019;394:1929–39.
5 Horn L, Mansfield AS, Szczęsna A, *et al*. First-line Atezolizumab plus chemotherapy in extensive-stage small-cell lung cancer. *N Engl J Med* 2018;379:2220–9.
6 Rudin CM, Awad MM, Navarro A, *et al*. Pembrolizumab or placebo plus etoposide and platinum as first-line therapy for extensive-stage small-cell lung cancer: randomized, double-blind, phase III KEYNOTE-604 study. *J Clin Oncol* 2020;38:2369–79.
7 Wang J, Zhou C, Yao W, *et al*. Adebrelimab or placebo plus carboplatin and etoposide as first-line treatment for extensive-stage small-cell lung cancer (CAPSTONE-1): a Multicentre, randomised, double-blind, placebo-controlled, phase 3 trial. *Lancet Oncol* 2022;23:739–47.
8 Cheng Y, Han L, Wu L, *et al*. Effect of first-line Serplulimab vs placebo added to chemotherapy on survival in patients with extensive-stage small cell lung cancer: the ASTRUM-005 randomized clinical trial. *JAMA* 2022;328:1223–32.
9 Goldman JW, Dvorkin M, Chen Y, *et al*. Durvalumab, with or without Tremelimumab, plus platinum–etoposide versus platinum–etoposide alone in first-line treatment of extensive-stage small-cell lung cancer (CASPIAN): updated results from a randomised, controlled, open-label, phase 3 trial. *Lancet Oncol* 2021;22:51–65.
10 Liu SV, Reck M, Mansfield AS, *et al*. Updated overall survival and PD-L1 subgroup analysis of patients with extensive-stage small-cell lung cancer treated with Atezolizumab, carboplatin, and etoposide (Impower133). *J Clin Oncol* 2021;39:619–30.
11 Paz-Ares L, Goldman JW, Garassino MC, *et al*. PD-L1 expression, patterns of progression and patient-reported outcomes (pros) with Durvalumab plus platinum-etoposide in ES-SCLC: results from CASPIAN. *Annals of Oncology* 2019;30:v928–9.
12 Gadgeel SM, Pennell NA, Fidler MJ, *et al*. Phase II study of maintenance Pembrolizumab in patients with extensive-stage small cell lung cancer (SCLC). *J Thorac Oncol* 2018;13:1393–9.
13 Chung HC, Piha-Paul SA, Lopez-Martin J, *et al*. Pembrolizumab after two or more lines of previous therapy in patients with recurrent or metastatic SCLC: results from the KEYNOTE-028 and KEYNOTE-158 studies. *J Thorac Oncol* 2020;15:618–27.
14 Ott PA, Elez E, Hiret S, *et al*. Pembrolizumab in patients with extensive-stage small-cell lung cancer: results from the phase IB KEYNOTE-028 study. *JCO* 2017;35:3823–9.
15 Owonikoko TK, Park K, Govindan R, *et al*. Nivolumab and Ipilimumab as maintenance therapy in extensive-disease small-cell lung cancer: Checkmate 451. *J Clin Oncol* 2021;39:1349–59.
16 Hellmann MD, Callahan MK, Awad MM, *et al*. Tumor mutational burden and efficacy of Nivolumab monotherapy and in combination with Ipilimumab in small-cell lung cancer. *Cancer Cell* 2018;33:853–61.
17 Alexandrov LB, Nik-Zainal S, Wedge DC, *et al*. Signatures of mutational processes in human cancer. *Nature* 2013;500:415–21.
18 Ready N, Hellmann MD, Awad MM, *et al*. First-line Nivolumab plus Ipilimumab in advanced non-small-cell lung cancer (Checkmate 568): outcomes by programmed death ligand 1 and tumor mutational burden as biomarkers. *J Clin Oncol* 2019;37:992–1000.
19 Rudin CM, Poirier JT, Byers LA, *et al*. Molecular subtypes of small cell lung cancer: a synthesis of human and mouse model data. *Nat Rev Cancer* 2019;19:289–97.
20 Gay CM, Stewart CA, Park EM, *et al*. Patterns of transcription factor programs and immune pathway activation define four major subtypes of SCLC with distinct therapeutic Vulnerabilities. *Cancer Cell* 2021;39:346–60.
21 Lim JS, Ibaseta A, Fischer MM, *et al*. Intratumoural heterogeneity generated by notch signalling promotes small-cell lung cancer. *Nature* 2017;545:360–4.
22 Tosi A, Parisatto B, Menegaldo A, *et al*. The immune Microenvironment of HPV-positive and HPV-negative oropharyngeal squamous cell carcinoma: a Multiparametric quantitative and spatial analysis unveils a rationale to target treatment-Naïve tumors with immune Checkpoint inhibitors. *J Exp Clin Cancer Res* 2022;41:279.
23 Qi J, Zhang J, Liu N, *et al*. Prognostic implications of molecular subtypes in primary small cell lung cancer and their correlation with cancer immunity. *Front Oncol* 2022;12:779276.
24 Baine MK, Hsieh M-S, Lai WV, *et al*. SCLC subtypes defined by Ascl1, Neurod1, Pou2F3, and Yap1: A comprehensive immunohistochemical and histopathologic characterization. *J Thorac Oncol* 2020;15:1823–35.
25 Ireland AS, Micinski AM, Kastner DW, *et al*. MYC drives temporal evolution of small cell lung cancer subtypes by Reprogramming Neuroendocrine fate. *Cancer Cell* 2020;38:60–78.
26 Lissa D, Takahashi N, Desai P, *et al*. Heterogeneity of Neuroendocrine transcriptional States in metastatic small cell lung cancers and patient-derived models. *Nat Commun* 2022;13:2023.
27 Bonanno L, Calvetti L, Dal Maso A, *et al*. Real-world impact of the introduction of Chemo-Immunotherapy in extended small cell lung cancer: a Multicentric analysis. *Front Immunol* 2024;15:1353889.
28 Moliner L, Zellweger NM, Schmidt SM, *et al*. 66P real-world data of first-line Chemo-Immunotherapy for patients with extensive stage SCLC: A Multicentre experience from Switzerland and the UK. *Immuno-Oncology and Technology* 2022;16:100171.
29 Farid S, Zhao S, Patel S, *et al*. Real world outcomes of patients treated with first line Chemo-Immunotherapy (IO) for small cell lung cancer (SCLC): impact of brain metastases and patterns of subsequent therapy. *JCO* 2023;41:e20639.
30 Wang Y, Mathai J, Alamgeer M, *et al*. Real-world analysis of clinical characteristics and survival outcomes in patients with extensive-stage SCLC treated with first-line Chemoimmunotherapy. *JTO Clinical and Research Reports* 2023;4:100544.
31 Busch SE, Hanke ML, Kargl J, *et al*. Lung cancer subtypes generate unique immune responses. *J Immunol* 2016;197:4493–503.
32 Chan JM, Quintanal-Villalonga Á, Gao VR, *et al*. Signatures of plasticity, metastasis, and immunosuppression in an Atlas of human small cell lung cancer. *Cancer Cell* 2021;39:1479–96.
33 Liu SV, Mok TSK, Nabet BY, *et al*. Clinical and molecular characterization of long-term survivors with extensive-stage small cell lung cancer treated with first-line Atezolizumab plus carboplatin and etoposide. *Lung Cancer* 2023;186:107418.
34 Nabet BY, Hamidi H, Lee MC, *et al*. Immune heterogeneity in small-cell lung cancer and vulnerability to immune Checkpoint blockade. *Cancer Cell* 2024;42:429–43.
35 Girault I, Adam J, Shen S, *et al*. APD-1/PD-L1 proximity assay as a Theranostic marker for PD-1 blockade in patients with metastatic Melanoma. *Clin Cancer Res* 2022;28:518–25.
36 Keir ME, Freeman GJ, Sharpe AH. PD-1 regulates self-reactive Cd8+ T cell responses to antigen in lymph nodes and Tissues1. *J Immunol* 2007;179:5064–70.
37 Dolina JS, Van Braeckel-Budimir N, Thomas GD, *et al*. Cd8+ T cell exhaustion in cancer. *Front Immunol* 2021;12:1–13.
38 Jiang W, He Y, He W, *et al*. Exhausted Cd8+T cells in the tumor immune Microenvironment: new pathways to therapy. *Front Immunol* 2020;11:622509.

J Immunother Cancer: first published as 10.1136/jitc-2024-008974 on 1 July 2024. Downloaded from http://jitc.bmj.com/ on December 31, 2024 by guest. Protected by copyright.

39 Miller BC, Sen DR, Al Abosy R, *et al*. Subsets of exhausted Cd8+ T cells Differentially mediate tumor control and respond to Checkpoint blockade. *Nat Immunol* 2019;20:326–36.
40 Liu B, Hu X, Feng K, *et al*. Temporal single-cell tracing reveals Clonal revival and expansion of precursor exhausted T cells during anti-PD-1 therapy in lung cancer. *Nat Cancer* 2022;3:108–21.
41 Dora D, Rivard C, Yu H, *et al*. Characterization of tumor-associated Macrophages and the immune Microenvironment in limited-stage Neuroendocrine-high and -Low small cell lung cancer. *Biology (Basel)* 2021;10:502.
42 Klein S, Schulte A, Arolt C, *et al*. Intratumoral abundance of M2-Macrophages is associated with unfavorable prognosis and markers of T-cell exhaustion in small cell lung cancer patients. *Mod Pathol* 2023;36:100272.
43 Forssell J, Oberg A, Henriksson ML, *et al*. High macrophage infiltration along the tumor front correlates with improved survival in colon cancer. *Clin Cancer Res* 2007;13:1472–9.
44 Christofides A, Strauss L, Yeo A, *et al*. The complex role of tumor-infiltrating Macrophages. *Nat Immunol* 2022;23:1148–56.
45 Li X, Liu J, Qian L, *et al*. Expression of Pfkfb3 and Ki67 in lung adenocarcinomas and targeting Pfkfb3 as a therapeutic strategy. *Mol Cell Biochem* 2018;445:123–34.
46 Vardhana SA, Hwee MA, Berisa M, *et al*. Impaired mitochondrial oxidative Phosphorylation limits the self-renewal of T cells exposed to persistent antigen. *Nat Immunol* 2020;21:1022–33.
47 Dimeloe S, Burgener AV, Grählert J, *et al*. T-cell metabolism governing activation, proliferation and differentiation; a modular view. *Immunology* 2017;150:35–44.
48 Kelly B, O'Neill LAJ. Metabolic Reprogramming in Macrophages and Dendritic cells in innate immunity. *Cell Res* 2015;25:771–84.
49 Stirling ER, Bronson SM, Mackert JD, *et al*. Metabolic implications of immune Checkpoint proteins in cancer. *Cells* 2022;11:1–22.
50 Chang C-H, Qiu J, O'Sullivan D, *et al*. Metabolic competition in the tumor Microenvironment is a driver of cancer progression. *Cell* 2015;162:1229–41.
51 Najjar YG, Menk AV, Sander C, *et al*. Tumor cell oxidative metabolism as a barrier to PD-1 blockade Immunotherapy in Melanoma. *JCI Insight* 2019;4:e124989.
52 Krencz I, Sztankovics D, Danko T, *et al*. Progression and metastasis of small cell lung carcinoma: the role of the Pi3K/AKT/mTOR pathway and metabolic alterations. *Cancer Metastasis Rev* 2021;40:1141–57.
53 Thirusangu P, Ray U, Sarkar Bhattacharya S, *et al*. Pfkfb3 regulates cancer Stemness through the Hippo pathway in small cell lung carcinoma. *Oncogene* 2022;41:4003–17.
54 Ando S, Perkins CM, Sajiki Y, *et al*. mTOR regulates T cell exhaustion and PD-1–targeted Immunotherapy response during chronic viral infection. *J Clin Invest* 2023;133:e160025.
55 Pasello G, Pigato G, Lorenzi M, *et al*. Cell-free (CF) DNA as predictive biomarker (B) of treatment outcome in extensive small cell lung cancer (eSCLC) patients (Pts) receiving Atezolizumab, carboplatin and etoposide (ACE): CATS/MI43257 study. *Annals of Oncology* 2023;34:S1074.
56 Pasello G, Urso L, Cavallari I, *et al*. Circulating Micro Rnas (cmiRNAs) as treatment outcome predictors in extensive small cell lung cancer (eSCLC) patients (Pts) receiving Atezolizumab plus carboplatin and etoposide (ACE): CATS/MI43257 study. *Annals of Oncology* 2023;34:S1073–4.

J Immunother Cancer: first published as 10.1136/jitc-2024-008974 on 1 July 2024. Downloaded from http://jitc.bmj.com/ on December 31, 2024 by guest. Protected by copyright.

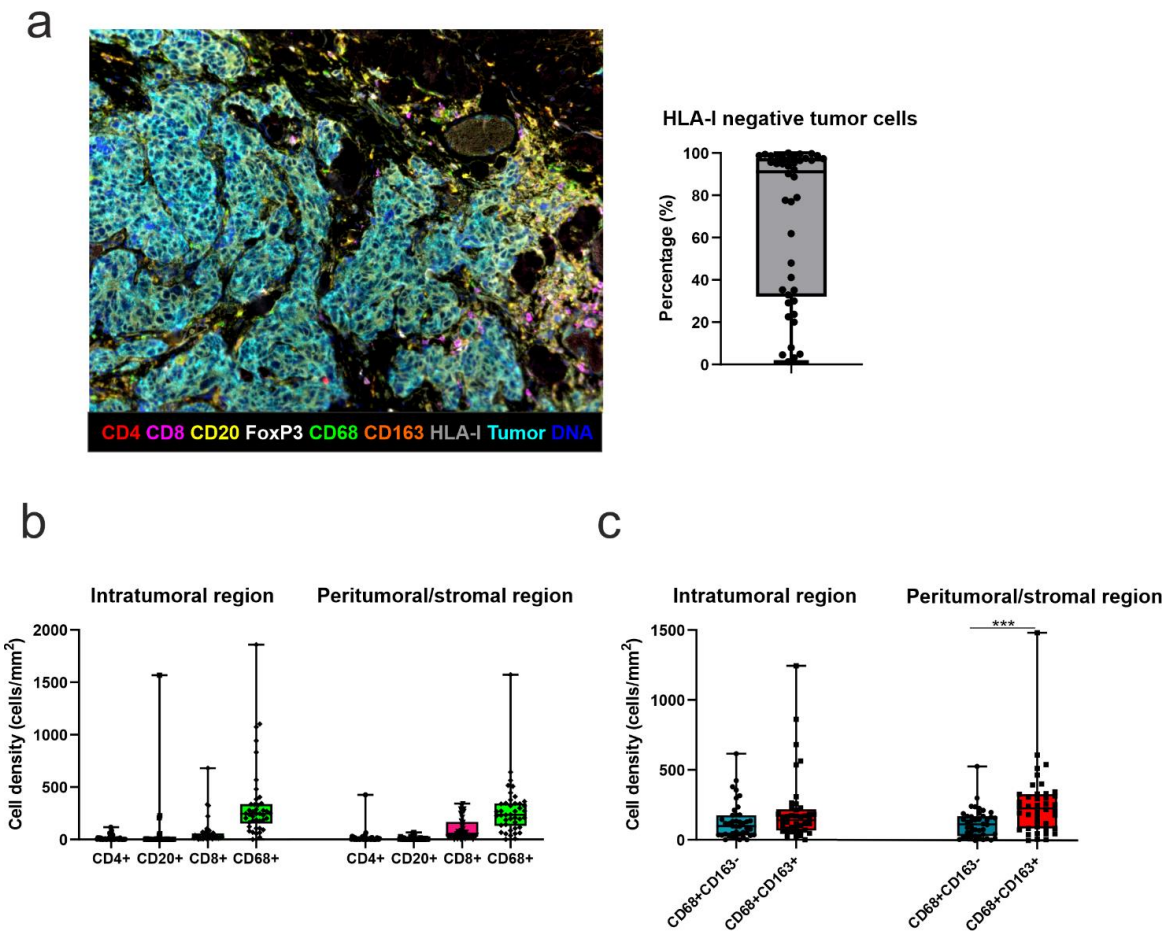

Supplementary Figure 1. Immune microenvironment characterization. a) Left: Representative image of ES-SCLC sample stained with the first mIF panel. Markers and color codes are delineated under the picture. Original magnification x20. Right: Percentage of HLA-class I negative tumor cells in ES-SCLC samples. b) Quantification of immune cells infiltrating the ES-SCLC microenvironment. c) Quantification of M1-like (CD68+CD163-) and M2-like (CD68+CD163+) macrophages infiltrating the ED-SCLC microenvironment.

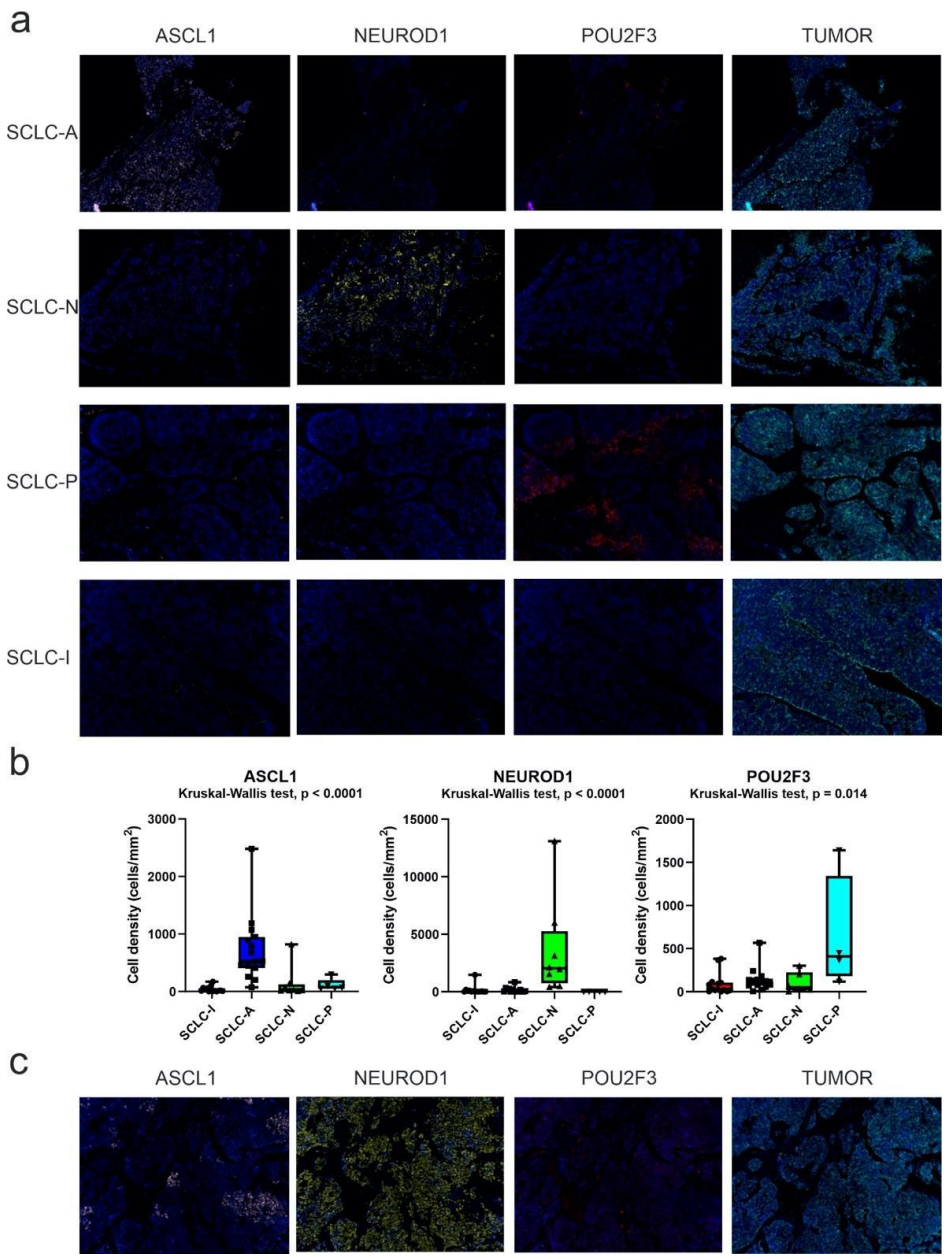

Supplementary Figure 2. Identification of four SCLC subtypes. a) Four SCLC subtypes were identified by mIF according to the differential expression of the transcription factors ASCL1, NEUROD1 and POU2F3. b) Quantification by mIF of ASCL1, NEUROD1 and POU2F3 transcription factors in SCLC subtypes. c) Representative images of the co-expression of different transcription factors by tumor cells within the same SCLC sample. Original magnification x20.

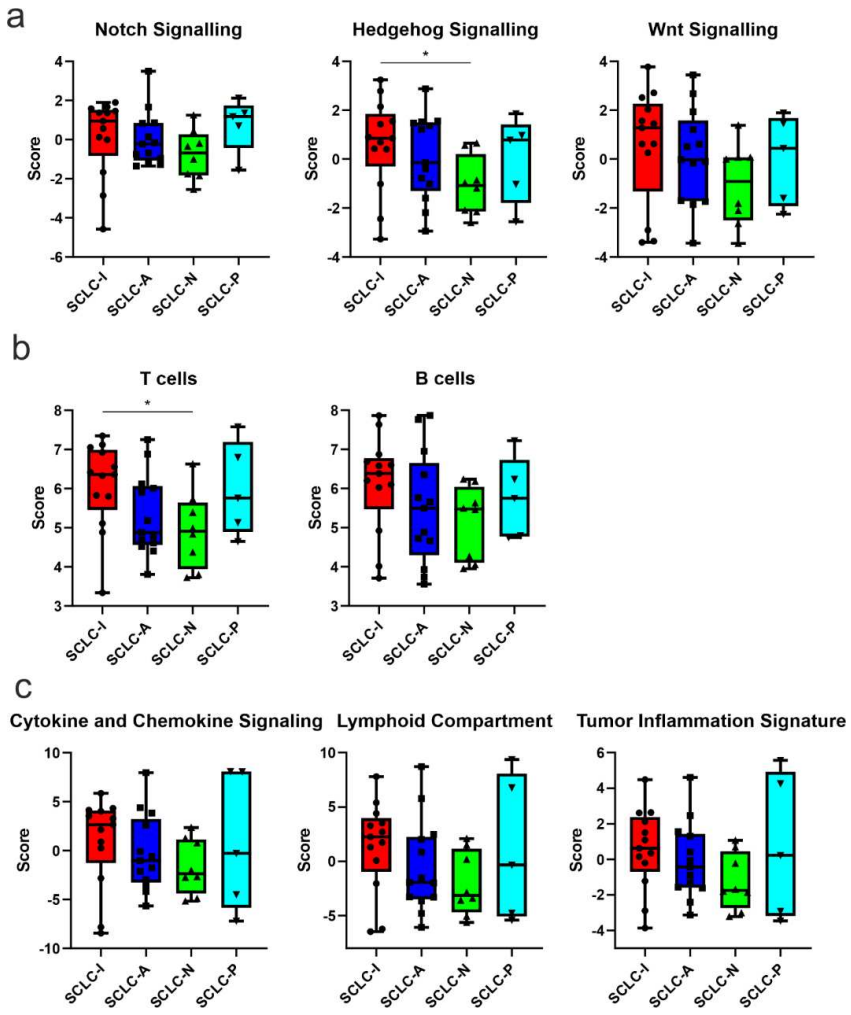

Supplementary Figure 3. Gene-based signalling analysis in SCLC subtypes.

Supplementary Table 1. mIF first panel

Primary antibody	Clone	Vendor	Cell population
CD68	KP1	Agilent	Pan-macrophages
CD8	C8/144B	Agilent	Cytotoxic T cells
FoxP3	D2W8E	Cell Signalling	T regulatory cells (CD4+FoxP3+)
CD4	4B12	Thermo Fisher Scientifics	T helper lymphocytes
CD20	L26	Agilent	B lymphocytes
CD163	10D6	Leica Biosystems	M2-like macrophages (CD68+CD163+)
HLA-I	EMR8-5	Abcam	Human leukocyte antigen-class I
Synaptophysin Chromogranin-A NCAM	27G12 5H7 123C3	Leica Biosystems Leica Biosystems Agilent	Tumor cells

Supplementary Table 2. mIF second panel

Primary antibody	Clone	Vendor	Cell population
PD-1	EPR4877-2	Abcam	Exhausted T cells (CD8+PD-1+)
PD-L1	E1L3N	Cell Signalling	Immunosuppressive cells
CD68	KP1	Agilent	Pan-macrophages
CD8	C8/144B	Agilent	Cytotoxic T cells
ASCL1	24B72D11.1	Becton Dickinson	SCLC-A subtype
NEUROD1	EPR20766	Abcam	SCLC-N subtype
POU2F3	Polyclonal	BioTechne	SCLC-P subtype
Synaptophysin Chromogranin-A NCAM	27G12 5H7 123C3	Leica Biosystems Leica Biosystems Agilent	Tumor cells

Supplementary table 3. Univariate and multivariate analysis for TTF (Log-rank and cox proportional hazard)

			Univariate analysis	Multivariate analysis TTF		
Variable	***N* (%)**		***p***	**Coefficient**	***P***	**HR (95% CI)**
Number of cases	42	(100.0)				
Gender						
Male	25	(59.5)	**0.032**			
Female	17	(40.5)		-1.040	0.090	0.353 (0.106 - 1.177)
Age						
< 68	20	(47.6)	0.226	0.741	0.383	0.512 (0.122-2.149)
>/= 68	22	(52.4)				
Smoking status						
Never smokers	3	(7.2)	0.170	-2.101	0.075	0.122 (0.012-1.232)
Smokers	39	(92.8)				
Stage at diagnosis						
IIIC/IVA	5	(11.9)	0.390	0.741	0.390	2.098 (0.396 - 11.110)
IVB	37	(88.1)				
ECOG PS						
0-1	34	(81.0)	0.260	-0.598	0.492	0.550 (0.100 - 3.023)
≥2	8	(9.0)				
Charlson Comorbidity Index						
6-7	12	(28.6)	0.074	1.280	0.091	3.598 (0.816 - 15.863)
>7	30	(71.4)				
Number of metastatic sites at diagnosis						
<3	27	(64.3)	**0.001**			
≥3	15	(35.7)		**1.491**	**0.044**	**4.440 (1.043 - 18.910)**
Brain metastasis at diagnosis						
Present	12	(28.6.)	0.467	0.157	0.764	1.170 (0.421 - 3.252)
Absent	30	(71.4)				
Liver metastasis at diagnosis						
Present	18	(42.9)	0.189			
Absent	24	(57.1)		-0.325	0.597	0.723 (0.217 - 2.409)
Steroid therapy at treatment start						
No	23	(54.7)	**0.007**	**-1.588**	**0.019**	**0.204 (0.0543 - 0.769)**
Yes	19	(45.2)				
Antibiotic therapy at treatment start						
No	37	(88.1)	0.314			
Yes	5	(10.2)		0.0632	0.946	1.065 (0.172 - 6.586)

Abbreviations: N, number; HR, hazard ratio; CI, confidence interval; PD, performance status; TTF, time-to-treatment failure..

Supplementary Table 4. Univariate and multivariate analysis for PFS (Log-rank and cox proportional hazard)

			Univariate analysis	Multivariate analysis PFS		
Variable	***N* (%)**		***p***	**Coefficient**	***P***	**HR (95% CI)**
Number of cases	42	(100.0)				
Gender						
Male	25	(59.5)	**0.014**	**-1.381**		
Female	17	(40.5)			**0.026**	**0.251 (0.0744 - 0.850)**
Age						
< 68	20	(47.6)	0.121	0.280	0.564	1.323 (0.322 - 5.432)
>/= 68	22	(52.4)				
Smoking status						
Never smokers	3	(7.2)	0.101	-1.978	0.090	0.138 (0.0141 - 1.358)
Smokers	39	(92.8)				
Stage at diagnosis						
IIIC/IVA	5	(11.9)	0.333	0.669	0.436	1.953 (0.362 - 10.525)
IVB	37	(88.1)				
ECOG PS						
0-1	34	(81.0)	0.422	-1.094	0.201	0.335 (0.0628 - 1.788)
≥2	8	(9.0)				
Charlson Comorbidity Index						
6-7	12	(28.6)	0.187	0.406	0.564	1.501 (0.377 - 5.973)
>7	30	(71.4)				
Number of metastatic sites at diagnosis						
<3	27	(64.3)	**0.001**	0.379		
≥3	15	(35.7)			0.591	1.461 (0.367 - 5.819)
Brain metastasis at diagnosis						
Present	12	(28.6.)	0.365	0.186	0.710	1.205 (0.451 - 3.221)
Absent	30	(71.4)				
Liver metastasis at diagnosis						
Present	18	(42.9)	0.491	-0.155		
Absent	24	(57.1)			0.770	0.856 (0.302 - 2.430)
Steroid therapy at treatment start						
No	23	(54.7)	**0.061**	**-1.440**	**0.022**	**0.237 (0.0691 - 0.813)**
Yes	19	(45.2)				
Antibiotic therapy at treatment start						
No	37	(88.1)	0.201	-0.763		
Yes	5	(10.2)			0.419	0.466 (0.073 - 2.962)

Abbreviations: N, number; HR, hazard ratio; CI, confidence interval; PD, performance status, PFS, progression-free survival.

Supplementary table 5. Univariate and multivariate analysis for OS (Log-rank and cox proportional hazard)

			Univariate analysis	Multivariate analysis OS		
Variable	***N* (%)**		***p***	**Coefficient**	***P***	**HR (95% CI)**
Number of cases	42	(100.0)				
Gender						
Male	25	(59.5)	0.071	-0.904		
Female	17	(40.5)			0.151	0.405 (0.118 - 1.390)
Age						
< 68	20	(47.6)	0.704	-0.738	0.319	0.478 (0.112 - 2.042)
>/= 68	22	(52.4)				
Smoking status						
Never smokers	3	(7.2)	0.160	-2.995	0.016	0.0500 (0.004 - 0.573)
Smokers	39	(92.8)				
Stage at diagnosis						
IIIC/IVA	5	(11.9)	0.247	-1.577	0.112	0.207 (0.023 - 1.447)
IVB	37	(88.1)				
ECOG PS						
0-1	34	(81.0)	**0.009**	**-1.891**	**0.053**	**0.151 (0.022 - 1.027)**
≥2	8	(9.0)				
Charlson Comorbidity Index						
6-7	12	(28.6)	0.800	-0.152	0.837	0.859 (0.200 - 3.682)
>7	30	(71.4)				
Number of metastatic sites at diagnosis						
<3	27	(64.3)	**<0.001**			
≥3	15	(35.7)		**1.943**	**0.007**	**6.981 (1.685 - 28.920)**
Brain metastasis at diagnosis						
Present	12	(28.6.)	0.347	0.650	0.258	1.916 (0.621 - 5.909)
Absent	30	(71.4)				
Liver metastasis at diagnosis						
Present	18	(42.9)	0.517	-1.243		
Absent	24	(57.1)			0.088	0.289 (0.069 - 1.202)
Steroid therapy at treatment start						
No	23	(54.7)	**0.011**	-0.908	0.142	0.403 (0.120 - 1.354)
Yes	19	(45.2)				
Antibiotic therapy at treatment start						
No	37	(88.1)	0.290	-1.187		
Yes	5	(10.2)			0.353	0.305 (0.025 - 3.737)
Response to treatment						
Responders	26	(61.9)	0.072	1.572		
Non-responders/ Not evaluated	16	(38.0)			0.023	4.816 (1.237 - 18.748)

Abbreviations: N, number; HR, hazard ratio; CI, confidence interval; PD, performance status; OS, overall survival.

Supplementary table 6. Multivariate analysis for TTF (a), PFS (b) and OS (c) including clinical features and biomarkers.

Variables		Coefficient	p
a. Multivariate for TTF			
	Exhausted CD8-related pathway	-2.16431	**0.00011**
	CD20+ cells	-1.12347	**0.03678**
	ASCL1+ tumor cells	-2.55669	**3.51e-05**
	Tumor cells within 20 μm from CD163+ macrophages (%)	0.90877	0.08766
	No steroid therapy at treatment start	-0.98979	0.06652
b. Multivariate for PFS			
	Exhausted CD8-related pathway	-1.9959	**0.000213**
	ASCL1+ tumor cells	-1.8617	**0.000720**
	No steroid therapy at treatment start	-1.3267	**0.007095**
	Male gender	1.0353	**0.041718**
b. Multivariate for OS			
	CD20+ cells	-1.0495	0.065873
	ASCL1+ tumor cells	-2.1548	**0.000305**
	POU2F3+ cells	1.7535	**0.003566**
	CD8 T cells within 20 μm from CD4 T cells	-1.5487	**0.005276**
	Less than 3 metastatic sites	-1.0442	**0.047800**

Abbreviations: PFS, progression-free survival; TTF, time to treatment failure; OS, overall survival; CD cluster of differentiation;

mIF staining

For each marker, the staining conditions were optimized using monoplex-stained slides of positive control tissues and then re-examined on a multiplex-stained ES-SCLC slide. Prior to staining, all 4 µm thick FFPE tissue sections were deparaffinized by overnight baking at 56°C, immersion in BOND Dewax Solution at 72°C and rehydration in ethanol. Heat-induced epitope retrieval pretreatments were performed using BOND Epitope Retrieval (ER) Solutions citrate-based pH 6.0 ER1 or EDTA-based pH 9.0 ER2 (both Leica Biosystems), depending on the primary antibody. Tissue sections were blocked with serum-free block/antibody diluent (Akoya Biosciences) for 10 minutes prior to the application of each primary antibody. The anti-mouse+rabbit horseradish peroxidase (HRP)-conjugated secondary antibody (Akoya Biosciences) was added for 10 minutes at room temperature, followed by incubation with different TSA-conjugated fluorophores for 10 minutes. Finally, spectral DAPI (Akoya Biosciences) was used as a nuclear counterstain and slides were mounted in ProLong Diamond Anti-fade Mountant (Life Technologies).